Generation of Fabry–Pérot oscillations and Dirac state in two-dimensional topological insulators by gate voltage*

Bin Xu(徐斌)[1,†], Rao Li(李饶)[2], and Hua-Hua Fu(傅华华)[3]

[1] Department of Mathematics and Information Sciences, North China university of Water Resources and Electric Power, Zhengzhou 450011, China
[2] Henan Mechanical and Electrical Vocational College, Zhengzhou 451191, China
[3] School of Physics, Huazhong University of Science and Technology, Wuhan 430074, China

(Received 5 December 2016; revised manuscript received 5 February 2017; published online 6 April 2017)

We investigate electron transport through HgTe ribbons embedded by strip-shape gate voltage through using a non-equilibrium Green function technique. The numerical calculations show that as the gate voltage is increased, an edge-related state in the valence band structure of the system shifts upwards, then hangs inside the band gap and merges into the conduction band finally. It is interesting that as the gate voltage is increased continuously, another edge-related state in the valence band also shifts upwards in the small-k region and contacts the previous one to form a Dirac cone in the band structure. Meanwhile in this process, the conductance spectrum displays as multiple resonance peaks characterized by some strong antiresonance valleys in the band gap, then behaves as Fabry–Pérot oscillations and finally develops into a nearly perfect quantum plateau with a value of $2e^2/h$. These results give a physical picture to understand the formation process of the Dirac state driven by the gate voltage and provide a route to achieving particular quantum oscillations of the electronic transport in nanodevices.

Keywords: Fabry–Pérot oscillations, Diarc cone, electronic transport, HgTe quantum well

PACS: 73.63.Hs, 73.23.–b, 73.20.At **DOI:** 10.1088/1674-1056/26/5/057303

1. Introduction

The quantum spin Hall (QSH) effect, which has been regarded as a class of topological state in two-dimensional (2D) materials, has attracted extensive attention due to its potential device applications in future low-consumption technology and information transport science.[1–4] The QSH effect was first predicted in some 2D models with honeycomb geometry, and then confirmed in HgTe/CdTe quantum wells (QWs) experimentally.[5] To obtain new exotic quantum states and to push the topological edge states towards practical device applications with particular functionalities, we should explore feasible routes to generating and operate the topological edge states. For example, by using magnetic doping in a topological insulator such as (Bi, Sb)$_2$Te$_3$, the quantum anomalous Hall state has been realized experimentally for the first time.[6] By applying an external magnetic field, the controllable spin polarized transport in HgTe QWs can be realized, and due to the Aharonov–Bohm effect, the quantum anomalous Hall-like phase has been observed, supporting that the relevant material can work as a spin filter.[7] Meanwhile, we can create and develop topological edge states artificially in some 2D materials. For example, by constructing a line defect in a graphene nanoribbon, two new quantum conduction channels, which can behave as two topological edges, appear along both sides of the linear defect, and the quantum states in the channels can be controlled by tuning the gate voltage embedded below the line defect.[8] If Anderson impurities are produced in HgTe QWs, it is found that the disorder can induce topological edge states.[9] Additionally, by embedding a top gate voltage on the surface of HgTe QWs, the transport behaviors of the topological edge states can be operated by adjusting the gate voltage, which provides a feasible way to fabricate topological field-effect transistors.[10]

Although there are many proposals and experimental designs to realize topological edge states, there is still less literature to analyze in detail how a general quantum state in some 2D materials is developed into topological ones, and also how the electron transport changes from an insulator state to a quantum topological one. In the end, we take a HgTe nanoribbon with a top gate voltage for example to demonstrate the detailed process of the formation of topological edge states. Our theoretical results show that as the gate voltage increases, an edge-related band state in the valence band shifts upwards, then hangs inside the bulk gap and finally merges into the conduction band to form a Dirac cone in the band structure. In this process, the conductance spectrum first shows strong antiresonance, then develops into Fabry–Pérot oscillations, and as the gate voltage is increased further to larger ones, a nearly perfect conductance plateau with a quantum value of $2e^2/h$ appears and behaves as the typical transport properties of topological edge states. The reminder of the paper is organized as follows. In Section 2, we introduce the Hamiltonian model of the sys-

*Project supported by the National Natural Science Foundation of China (Grant Nos. U1404108, 11104072, and 10947162) and Henan Foundation and Frontier Technology Research Program of China (Grant No. 162300410056).

†Corresponding author. E-mail: hnsqxb@163.com

© 2017 Chinese Physical Society and IOP Publishing Ltd

tem and the theoretical method. In Section 3, we present the numerical results to show the influences of the top gate voltage on the band structure and the formation of the Fabry–Pérot oscillations. Finally, we summarize our results in Section 4.

2. Device model and theoretical method

In the device design, a tripe-shape gate voltage is embedded on the surface of the HgTe ribbon as shown in Fig. 1(a), and the ribbon width is adopted as $L_y = Na$, where a (= 5 nm) is the lattice constant and N denotes the number of lattices in width. To eliminate the influence of the helical edge states located in both physical edges of the ribbon, we construct another HgTe model with a cylindrical geometry as drawn in Fig. 1(b). In this example, no topological edge states appear, if neither line defect nor disorder is produced.[9] To establish the Hamiltonian model, we consider a square lattice with four special orbit states, i.e., $|\mathrm{s},\uparrow\rangle$, $|\mathrm{p}_x+\mathrm{i}\mathrm{p}_y,\uparrow\rangle$, $|\mathrm{s},\downarrow\rangle$, and $|-(\mathrm{p}_x-\mathrm{i}\mathrm{p}_y),\downarrow\rangle$, on each lattice site. Here $\uparrow$ and $\downarrow$ denote the spin-up and spin-down components. Considering the symmetry in s and p orbitals, the effective Hamiltonian can be written as[11,12]

$$
\begin{aligned}
H = & \sum_{\boldsymbol{i}} \varphi_{\boldsymbol{i}}^{\dagger} \begin{pmatrix} E_{\boldsymbol{i}\mathrm{sa}} & 0 & 0 & 0 \\ 0 & E_{\boldsymbol{i}\mathrm{pc}} & 0 & 0 \\ 0 & 0 & E_{\boldsymbol{i}\mathrm{sb}} & 0 \\ 0 & 0 & 0 & E_{\boldsymbol{i}\mathrm{pd}} \end{pmatrix} \varphi_{\boldsymbol{i}} \\
& + \sum_{\boldsymbol{i}} \varphi_{\boldsymbol{i}}^{\dagger} \begin{pmatrix} V_{\mathrm{ss}} & V_{\mathrm{sp}} & 0 & 0 \\ -V_{\mathrm{sp}}^{*} & V_{\mathrm{pp}} & 0 & 0 \\ 0 & 0 & V_{\mathrm{ss}} & V_{\mathrm{sp}}^{*} \\ 0 & 0 & -V_{\mathrm{sp}} & V_{\mathrm{sp}} \end{pmatrix} \varphi_{\boldsymbol{i}+\delta x} + \mathrm{H.c.} \\
& + \sum_{\boldsymbol{i}} \varphi_{\boldsymbol{i}}^{\dagger} \begin{pmatrix} V_{\mathrm{ss}} & \mathrm{i}V_{\mathrm{sp}} & 0 & 0 \\ \mathrm{i}V_{\mathrm{sp}}^{*} & V_{\mathrm{pp}} & 0 & 0 \\ 0 & 0 & V_{\mathrm{ss}} & -\mathrm{i}V_{\mathrm{sp}}^{*} \\ 0 & 0 & -\mathrm{i}V_{\mathrm{sp}} & V_{\mathrm{pp}} \end{pmatrix} \varphi_{\boldsymbol{i}+\delta y} + \mathrm{H.c.} \quad (1)
\end{aligned}
$$

Here $\boldsymbol{i} = (ix, iy)$ is the site index, and δx and δy are the unit vectors along the length (x) and width (y) direction, and $\varphi_{\boldsymbol{i}} = (a_i, c_i, b_i, d_i)^{\mathrm{T}}$ represents the four annihilation operators of electron on the lattice $\boldsymbol{i}$. If the gate voltage is not taken into account, the on-site potentials are set to be $E_{\boldsymbol{i}\mathrm{sa}} = E_{\boldsymbol{i}\mathrm{sb}} = E_{\mathrm{s}}$ and $E_{\boldsymbol{i}\mathrm{pc}} = E_{\boldsymbol{i}\mathrm{pd}} = E_{\mathrm{p}}$, where E_{s}, E_{p}, V_{ss}, V_{pp}, and V_{sp} are the five independent parameters which characterize the clean HgTe sample. Considering that the top gate is covered on some lattice sites, the corresponding on-site potentials should be added by the voltage strength V_{g}. It is clear that near the Γ point, the lattice Hamiltonian in k representation can be reduced to the continuous Hamiltonian,[13] when we take $V_{\mathrm{sp}} = -\mathrm{i}A/2a$, $V_{\mathrm{ss}} = (B+D)/a^2$, $V_{\mathrm{pp}} = (D-B)/a^2$, $E_{\mathrm{s}} = C + M - 4(B+D)/a^2$, and $E_{\mathrm{p}} = C - M - 4(D-B)/a^2$, where the parameters A, B, C, D, and M can be drawn from the relevant experimental results.[5]

To calculate the linear conductance of the HgTe ribbon, the Landauer–Büttiker formula is used,[13] thus the conductance of the ribbon at zero temperature and low bias voltage can be expressed as $G_{\mathrm{LR}} = \frac{e^2}{h}\mathrm{Tr}[\mathrm{Re}(\Gamma_{\mathrm{L}} G^r \Gamma_{\mathrm{R}} G^a)]$, where $\Gamma_{\mathrm{L/R}}$ describes the coupling between the left/right semi-infinite lead and the central region, and it is expressed as $\Gamma_{\mathrm{L/R}} = \mathrm{i}(\Sigma^{\mathrm{r}}_{\mathrm{L/R}} - \Sigma^{\mathrm{a}}_{\mathrm{L/R}})$.[14,15] Here $\Sigma^{\mathrm{r}}_{\mathrm{L/R}} = h_{(\mathrm{L/R})\mathrm{C}} g_{\mathrm{L/R}} h^{\dagger}_{(\mathrm{L/R})\mathrm{C}}$ is the retarded self-energy due to the fact that each of the lead L (or R) and $\Sigma^{\mathrm{a}}_{\mathrm{L/R}}$ is the advanced self-energy, $h_{(\mathrm{L/R})\mathrm{C}}$ is the hopping from the lead L (or R) to the central region C, and $g_{\mathrm{L/R}} = (E - H_{\mathrm{L/R}})^{-1}$ is the Green function of the lead or drain, where $H_{\mathrm{L/R}}$ is the Hamiltonian of the left (or right) lead. In the previous expression, $G^{\mathrm{r/a}} = (E - H_{\mathrm{C}} - \Sigma^{\mathrm{r/a}}_{\mathrm{L}} - \Sigma^{\mathrm{r/a}}_{\mathrm{R}})^{-1}$ is the retarded Green function,[16–18] and H_{C} is the Hamiltonian for the central scattering region. For the detailed numerical calculations, one can refer to Ref. [9].

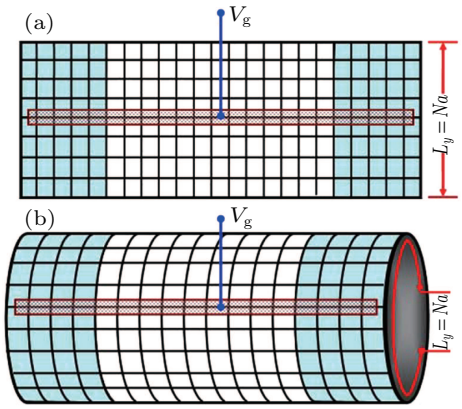


Fig. 1. (color online) Schematics of HgTe nanoribbon in (a) open boundary condition and (b) periodic boundary condition in the width (L_y) direction. The source and drain exist in the (pale green) filled regions. In both devices, a top gate voltage (a long trip shape) is embedded on the surface of the HgTe sample in the transport direction. The width of the ribbon and the circumference of the cylinder are set to be $L_y = Na$, where a is the lattice constant and N is the corresponding number of the lattices in the width direction.

3. Results and discussion

Firstly, we present the band structure of a clean HgTe nanoribbon with a cylindrical geometry, in which the circumference is set to be $L_y = 80a$ (i.e., 400 nm) and the top gate is placed on the 40st lattice site along the transport direction, as shown in Fig. 1(b). Figures 2(a)–2(g) show the numerical results as the gate voltage V_{g} is increased from zero to 1.4 eV. For $V_{\mathrm{g}} = 0$, the band shows a bulk gap of approximately $2|M|$, displaying a good insulator characteristic.[19,20] When a finite and small voltage is applied, for example $V_{\mathrm{g}} = 30$ meV, we find that an edge-related state (red line) in the valance band shifts upwards while keeping gapless at the point of $k_x = 0$. Besides these, other band lines nearly do not show any changes (Fig. 2(b)). When V_{g} is tuned to 50 meV, the edge-related state develops into a localized one and hangs inside the bulk gap (Fig. 2(c)). As V_{g} is increased further, the hanging state shifts upwards continuously and merges into the conduction band as shown in Figs. 2(d) and 2(e). In this process, it is inter-

esting that another edge-related state in the valence band also shifts upwards (Figs. 2(c)–2(g)). Nevertheless, this shifting tendency occurs only in the small-k_x region, which is very different from the previous one. When V_g is further increased to a large one, for example $V_g = 1.4$ eV, the new-developed edge-related state in the valence band nearly contacts the previous one at $k_x = 0$, displaying as a linear Dirac-type characteristic. To make a comparison with the topological edge state of HgTe nanoribbons predicted by Bernevig *et al.*,[4] we calculate the band structure of the HgTe nanoribbon with open boundary conduction in width as shown in Fig. 2(h). Obviously, the new-developed edge states in the HgTe cylinder possess the same characteristics as those of the helical edge states in the HgTe nanoribbon with open boundary conditions in width, indicating that they have the same nature in physics.

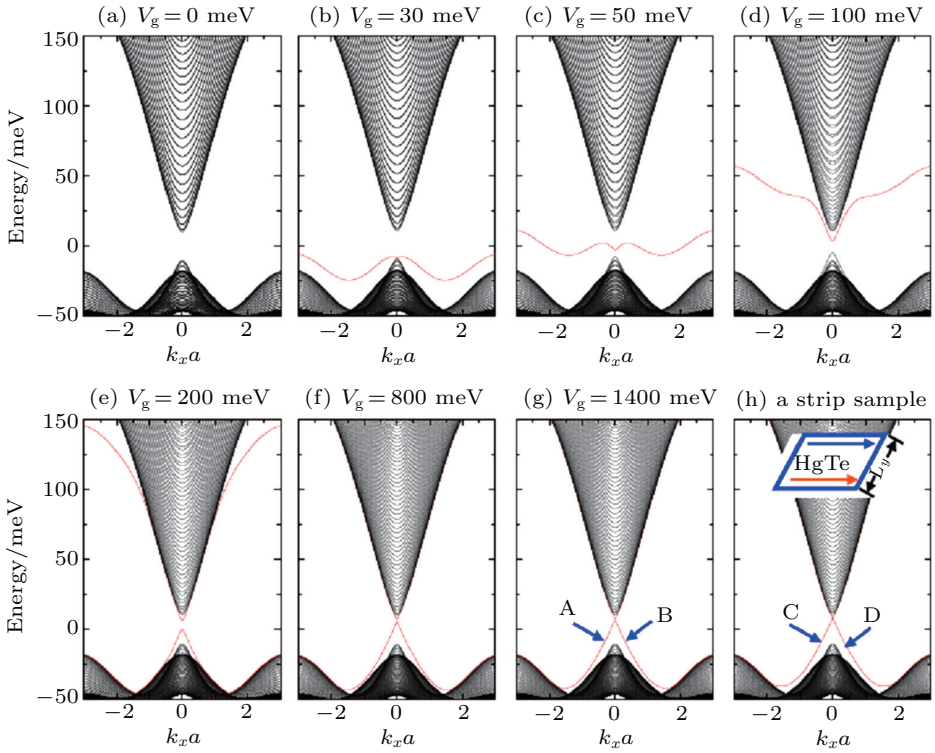


Fig. 2. (color online) (a)–(g) Band structures of the HgTe cylinder, where the periodic boundary condition in the width direction is used and the strip-shape gate voltage V_g is changed from 0 to 1400 meV. (h) Band structure of the HgTe nanoribbon in the open periodic boundary condition in the width direction. States A–D are some chosen states inside the bulk gap.

To obtain a better understanding of the new-developed edge states in the HgTe cylinder, we turn to the examination of their wave function distributions in real space. For the state A and B appearing inside the bulk gap in Fig. 2(g), the relevant wave function distributions across the width direction are plotted in Fig. 3(a). We find that the states A and B are associated just with the bound states at the 39st site and the 41st site respectively as shown in the inset of Fig. 3(a). More importantly, the wave function distributions of the edge states are nearly zero at the 40st site (see Fig. 3(b)), which corresponds exactly to the lattices covered by the gate voltage. Thus, it can be concluded that the lattices adjacent to the top gate mainly contribute to the new-developed edge states and construct the new quantum transport channels. Moreover, further numerical calculations show that the bound states in the quantum channels adjacent to the top gate are independent of the widths of the gate strip and the HgTe sample, indicating their stabilities. To examine the difference between the bound states in the new quantum channels and the helical edge states in the HgTe nanoribbon, we plot the wave function distributions of the state C and D in Fig. 3(c). As expected, the bound states in the new quantum channel nearly do not show any difference from the helical edges states in the HgTe ribbon. It can be believed that the new-developed edge states adjacent to the gate have the same characteristics of the quantum spin Hall effect.

Next, we turn our attention to the influence of the bound state developed by the top gate voltage on the conductance of the HgTe cylinder. For $V_g = 0$, one can see that the conductance spectrum exhibits an insulator-trivial feature with a full bulk gap $E_g = 2|M|$, which is consistent with the corresponding band structure (see Fig. 2(a)). As V_g is increased to 30 meV, in the conductance spectrum there appear two new peaks at $E = -8.8$ and -7.5 meV, respectively. These two peaks originate from the extended states in the valence band, marked by the red line in Fig. 2(b). As V_g is increased continuously to 50 meV, the conductance spectrum becomes very different. In the bulk gap region, the conductance peaks are filled in, and display as two different kinds of quantum oscil-

lations. In the low-energy region (-10 meV $\leq E \leq 2.5$ meV), the conductance spectrum keeps finite values with some round conductance peaks, behaving as Fabry–Pérot oscillations.[21] While, in the high-energy region (2.5 meV $\leq E \leq 10$ meV), the conductance spectrum shows some sharp peaks, and between two nearest peaks, the conductance keeps zero. Moreover, in this energy region, the conductance does not show any interference effect but some strong antiresonances. These interesting transport behaviors can be understood from the corresponding band structures plotted in Fig. 2(c). Obviously, there are some localized states (red line) hanging inside the bulk gap, and the localized states are closer to the valence band than to the conduction band. This property leads to two different types of quantum resonances in the conductance in the bulk gap as shown in Fig. 4(c). However, as V_g increases to 100 meV, the conductance peaks are developed into a conductance plateau in the high-energy region (3 meV $\leq E \leq 10$ meV), and in the low-energy region (-10 meV $\leq E \leq -4.8$ meV), some resonance peaks remain unchanged, while in the other region of the bulk gap, the conductance is suppressed to zero. With further increasing V_g, three typical transport characteristics appear: (i) all conductance peaks are developed into conductance plateaus near to the quantum value of $2e^2/h$; (ii) the gap between the peaks becomes narrow, and is contributed partly by the finite-size effect of the cylinder; and (iii) as V_g is adopted as a large value, for example $V_g = 1.4$ eV, the conductance displays as regular multiple-step structures with the quantum values of $2ne^2/h$ ($n = 1, 2, 3, \ldots$) as shown in Fig. 4(g). To further explain the interesting conductance features for the HgTe cylinder covered by a high gate voltage, a direct comparison with the linear conductance of a HgTe nanoribbon becomes necessary. Figure 4(h) shows the conductance of the HgTe nanoribbon with the width $L_y = 400$ nm, while without any gate voltage. Obviously, apart from a narrow gap with zero conductance due to the finite-size effect, there is no other difference. These transport characteristics also support that the bound states in the new conductance channels behave with the same features as these of the helical edge states in a HgTe ribbon.

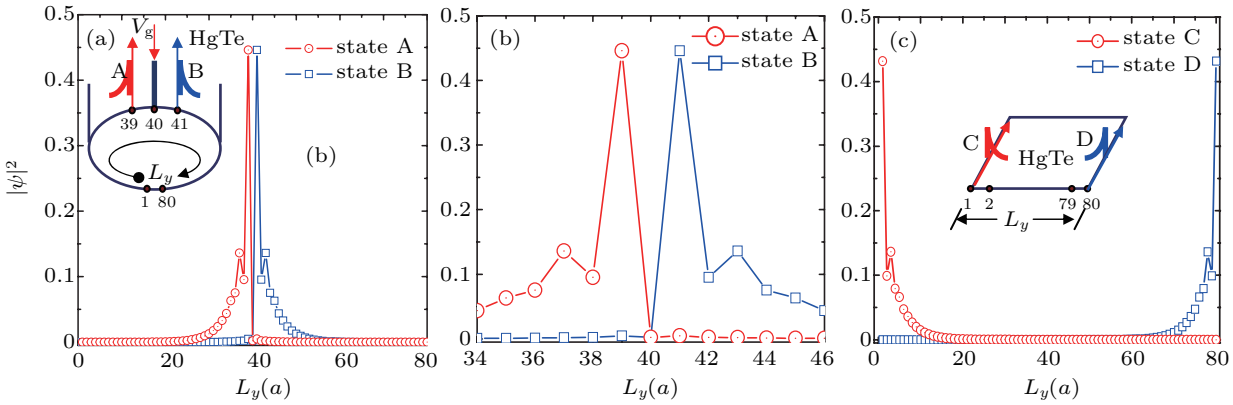


Fig. 3. (color online) (a) Wave function distributions of states A and B marked in Fig. 2(g) for the HgTe cylinder, where the gate voltage is applied to the 40st lattice site (see the inset), (b) the wave function distributions from the 35st to 45st lattice, (c) the wave function distributions of the states C and D labeled in Fig. 2(h) for a HgTe nanoribbon in open boundary conditions, while without any gate voltage, and the size of the sample is shown in the inset.

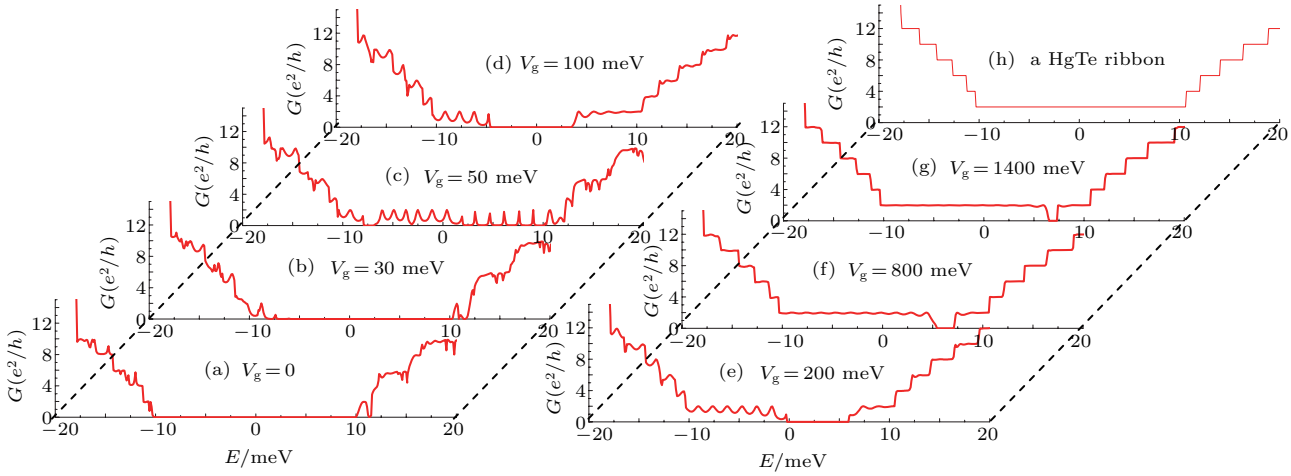


Fig. 4. (color online) (a)–(g) The conductances for the HgTe cylinder with the periodic boundary conditions, where the top gate voltage V_g is increased from zero to 1.4 eV. (h) The linear conductance for the HgTe nanoribbon in the open periodic boundary condition in the width direction.

4. Conclusions

In summary, we construct a HgTe sample with a cylinder configuration to show the formation of the topological edge states by applying a voltage to a strip-shaped top gate. The numerical results show that as the gate voltage increases, two bound states appear in the lattices adjacent to the gate and two transport channels are developed. Meanwhile in the band structures of the system, an edge-related quantum state shifts from the valence band, then behaves as a hanging state in the bulk gap, and as the gate voltage is increased further, the hanging state shifts upward continuously and merges into the conduction band. As the gate voltage is increased to a large one, a Dirac band forms in the bulk gap. Moreover, in this process, the conductance spectrum presents some resonance peaks with strong antiresonance in the band-gap region, then displays as Fabry–Pérot oscillations, and finally develops into a nearly perfect quantum plateau with a value of $2e^2/h$. These results give a physical picture to understand the detailed process of the formation of a Dirac cone produced by the gate voltage and provide a feasible route to the realization of particular quantum oscillations in the transport of topological edge states.

References

[1] Kane C L and Mele E J 2005 *Phys. Rev. Lett.* **95** 226801
[2] Fu L, Kane C L and Mele E J 2007 *Phys. Rev. Lett.* **98** 106803
[3] Wu C J, Bernevig B A and Zhang S C 2006 *Phys. Rev. Lett.* **96** 106401
[4] Bernevig B A, Hughes T H and Zhang S C 2006 *Science* **314** 1757
[5] König M, Wiedmann S, Brüne C, Roth A, Buhmann H, Molenkamp L W, Qi X L and Zhang S C 2007 *Science* **318** 766
[6] Chang C, Zhang J, Feng X, Shen J, Zhang Z, Guo M, Li K, Ou Y, Wei P, Wang L, Ji Z, Feng Y, Ji S, Chen X, Jia J, Dai X, Fang Z, Zhang S C, He K, Wang Y, Ma X and Xue Q K 2013 *Science* **340** 167
[7] Chen J, Wang J and Sun Q F 2012 *Phys. Rev. B* **85** 125401
[8] Song J, Liu H, Jiang H, Sun Q F and Xie X C 2012 *Phys. Rev. B* **86** 085437
[9] Jiang H, Wang L, Sun Q F and Xie X C 2009 *Phys. Rev. B* **80** 165316
[10] Fu H H, Gao J H and Yao K L 2014 *Nanotechnology* **25** 225201
[11] Li J, Chu R L Jain J K and Shen S Q 2009 *Phys. Rev. Lett.* **102** 136806
[12] Liu C X, Qi X L, Dai X, Fang Z and Zhang S C 2008 *Phys. Rev. Lett.* **101** 146802
[13] Datta S 1995 *Electronic Transport in Mesoscopic Systems* (Cambridge: Cambridge University Press)
[14] Chen J C, Wang J and Sun Q F 2012 *Phys. Rev. B* **85** 125401
[15] Xing Y, Sun Q F and Wang J 2006 *Phys. Rev. B* **73** 205339
[16] Fu H H, Yao K L and Liu Z L 2008 *J. Chem. Phys.* **129** 134706
[17] Fu H H, Yao K L and Liu Z L 2008 *J. Phys. Chem. A* **112** 6205
[18] Fu H H and Yao K L 2013 *Europhys. Lett.* **103** 57011
[19] Lee D H and Joannopoulos J D 1981 *Phys. Rev. B* **23** 4997
[20] Maciejko J, Liu C, Oreg Y, Qi X L, Wu C and Zhang S C 2009 *Phys. Rev. Lett.* **102** 256803
[21] Varlet A, Liu M H, Krueckl V, Bischoff D, Simonet P, Watanabe K, Taniguchi T, Richter K, Ensslin K and Ihn T 2014 *Phys. Rev. Lett.* **113** 116601